

# The circles-in-the-sky signature for three spherical universes

R. Aurich,<sup>1</sup> S. Lustig,<sup>1</sup> and F. Steiner<sup>1</sup>

<sup>1</sup>*Abteilung Theoretische Physik, Universität Ulm,  
Albert-Einstein-Allee 11, D-89069 Ulm, Germany*

## ABSTRACT

The mysteriously low CMB power on the largest scales might point to a Universe which consists of a multi-connected space. In addition to a suppression of large-scale power, a multi-connected space can be revealed by its circles-in-the-sky signature. In this paper, a detailed search for this signature is carried out for those three homogeneous multi-connected spherical space forms that lead to the smallest large-scale power. A simultaneous search for all occurring paired circles is made using filtered CMB sky maps which enhance the ordinary Sachs-Wolfe contribution. A marginal hint is found for the right-handed Poincaré dodecahedron at  $\Omega_{\text{tot}} \simeq 1.015$  and for the right-handed binary tetrahedral space at  $\Omega_{\text{tot}} \simeq 1.068$ . However, due to the complicated noise and foreground structure of the available microwave sky maps, we cannot draw firm conclusions from our findings.

**Key words:** cosmic microwave background - cosmic topology

## 1 INTRODUCTION

Current observational evidence strongly corroborates the standard big-bang model based on a Friedmann-Lemaître universe possessing a space-time structure  $\mathbb{R}_+ \times \mathcal{M}$ . Here  $\mathbb{R}_+$  describes cosmic time, and  $\mathcal{M}$  the three-dimensional co-moving space section of constant curvature  $K = +1, 0, -1$ . It is well-known that the Einstein field equations describe the local space-time geometry of the universe, once the spatial curvature  $K$  and the various mass/energy densities are given, but do not specify its global spatial geometry, i. e. its topology. Thus, in cosmology we are faced with two very fundamental questions:

- i) What is the value of  $K$ , i. e. the curvature of the universe?
- ii) What is the topology of the three-space  $\mathcal{M}$ ?

While the curvature does constrain the possible topologies, it does not fix it. Only if it is *assumed* that the space of the universe is simply-connected, the possible homogeneous three-spaces  $\mathcal{M}$  of constant curvature are given by the three-sphere  $\mathcal{S}^3(K = +1)$ , Euclidean three-space  $\mathcal{E}^3(K = 0)$ , or hyperbolic three-space  $\mathcal{H}^3(K = -1)$ . At present, there is, however, no compelling theoretical argument why the spatial geometry of the universe should be simply-connected, and thus we are confronted with the problem of “cosmic topology” (see Lachièze-Rey & Luminet (1995); Levin (2002) for a review).

The discovery of the temperature fluctuations  $\delta T$  of the cosmic microwave background (CMB) radiation by COBE

in 1992 (Smoot et al. 1992) and the detailed measurements by WMAP (Bennett et al. 2003) and by other groups offer an ideal testing ground for a study of cosmic topology. The first year WMAP data show a slight tendency to a positive curvature of the universe, at least within the  $1\sigma$ -band. In Aurich et al. (2005a) we have therefore carried out a systematic comparison of the WMAP data with the predictions obtained from a representative sample of homogeneous spherical space forms. As a result, we have found (Aurich et al. 2005a) that only three multi-connected spherical spaces are compatible with the observed CMB anisotropy. The most remarkable signature of these spherical universes is a suppression of the CMB power spectrum at large scales, in particular a large suppression of the CMB quadrupole and octopole, and of the temperature two-point correlation function on large angles (Luminet et al. 2003; Aurich et al. 2005b,a) in accordance with the COBE and WMAP measurements. It is worthwhile to emphasize that the suppression on large scales is a *prediction* of these universes and not put in by hand.

Multi-connected spaces can reveal themselves by the so-called circles-in-the-sky signature (Cornish et al. 1998). In this paper, we carry out a thorough search of these paired circles for the above mentioned three spherical spaces.

arXiv:astro-ph/0510847v1 31 Oct 2005

## 2 SPHERICAL FRIEDMANN-LEMAÎTRE UNIVERSES

In our search for the circles-in-the-sky signature in CMB sky maps, we are only interested in large-scale fluctuations of the CMB above horizon at recombination since these fluctuations should contain the fingerprint of a non-trivial topology. The observed relative temperature fluctuations  $\delta T/T = O(10^{-5})$  are very small, and thus it is sufficient to use linear perturbation theory. The four-dimensional space-time metric with scalar perturbations takes then the simple form (in conformal Newtonian gauge)

$$ds^2 = a^2(\eta) [(1 + 2\Phi)d\eta^2 - (1 - 2\Phi)|d\vec{x}|^2] \quad , \quad (1)$$

where  $\eta \in \mathbb{R}_+$  denotes the conformal time and  $a(\eta)$  the cosmic scale factor.  $|d\vec{x}|$  is the spatial distance on a given spherical space form  $\mathcal{M}$ . For vanishing  $\Phi$ ,  $\Phi \equiv 0$ , the metric (1) is the well-known Friedmann-Robertson-Walker metric. In writing the metric (1) with a non-vanishing scalar perturbation  $\Phi \neq 0$ , we have assumed that the energy-momentum tensor  $T_{\mu\nu}$  satisfies  $T_{ij} = 0$  for  $i \neq j$  ( $i, j = 1, 2, 3$ ) and that vector and tensor modes can be neglected in our study of the CMB.

In the following, we shall assume that the total energy density of the universe is given by a sum of 4 contributions: radiation, baryonic matter (bar), cold dark matter (cdm), and dark energy, where the latter is identified with a positive cosmological constant  $\Lambda$ . Then the scale factor  $a(\eta)$  is uniquely determined by the corresponding Friedmann equation.

Let us now discuss the geometry and topology of the spherical space forms. There are infinitely many spherical spaces which were classified by Threlfall & Seifert (1930, 1932) (see also Wolf (1974) and Gausmann et al. (2001)) and are given by the quotient  $\mathcal{M} = \mathcal{S}^3/\Gamma$  of the three-sphere  $\mathcal{S}^3$  under the action of a discrete fixed-point free subgroup  $\Gamma \subset \text{SO}(4)$  of the isometries of  $\mathcal{S}^3$ . To define the subgroup  $\Gamma$ , one makes use of the fact that the unit 3-sphere  $\mathcal{S}^3$  can be identified with the multiplicative, but non-commutative group of unit quaternions  $\{q\}$ . The latter are defined by  $q := w + xi + yj + zij$ ,  $(w, x, y, z) \in \mathbb{R}^4$ , having unit norm,  $|q|^2 = w^2 + x^2 + y^2 + z^2 = 1$ . Here, the 4 basic quaternions  $\{1, i, j, ij\}$  satisfy the multiplication rules  $i^2 = j^2 = -1$  and  $ij = -ji$  plus the property that  $i$  and  $j$  commute with every real number. The distance  $d(q_1, q_2)$  between two points  $q_1$  and  $q_2$  on  $\mathcal{S}^3$  is given by  $\cos d(q_1, q_2) = w_1 w_2 + x_1 x_2 + y_1 y_2 + z_1 z_2$ .

The group  $\text{SO}(4)$  is isomorphic to  $\mathcal{S}^3 \times \mathcal{S}^3 / \{\pm(1, 1)\}$ , and thus the subgroup  $\Gamma$  can act on the first  $\mathcal{S}^3$  factor, on the second  $\mathcal{S}^3$  factor or on both factors. Since we are only interested in orientable homogeneous manifolds  $\mathcal{M} = \mathcal{S}^3/\Gamma$ , we have to consider either right- or left-handed Clifford translations  $\gamma \in \Gamma$  that act on an arbitrary unit quaternion  $q \in \mathcal{S}^3$  by left-multiplication,  $q \rightarrow \gamma q$ , respectively, right-multiplication,  $q \rightarrow q\gamma$ . The right- (left-) handed Clifford translations act as right- (left-) handed cork screw translations.

Recently, we have carried out in Aurich et al. (2005a) a systematic comparison of the CMB anisotropy with the WMAP data for a representative sample of homogeneous spherical spaces and have found agreement with the data for 3 spaces only:  $\mathcal{T} := \mathcal{S}^3/I^*$ ,  $\mathcal{O} := \mathcal{S}^3/O^*$ , and  $\mathcal{D} := \mathcal{S}^3/I^*$ .

Here  $T^*$  denotes the binary tetrahedral group of order 24 generated by the right-handed Clifford translations  $\gamma_1 = j$  and  $\gamma_2 = (1 + i + j + ij)/2$ .  $O^*$  denotes the binary octahedral group of order 48 generated by the right-handed Clifford translations  $\gamma_1 = (1 + i)/\sqrt{2}$  and  $\gamma_2 = (1 + i + j + ij)/2$ . The last group  $I^*$  corresponding to the Poincaré dodecahedron  $\mathcal{D} = \mathcal{S}^3/I^*$  is the binary icosahedral group of order 120 and is generated by the right-handed Clifford translations  $\gamma_1 = j$  and  $\gamma_2 = (\sigma + \frac{1}{\sigma}i + j)/2$  with  $\sigma = (1 + \sqrt{5})/2$ . In addition to these 3 spaces there are the 3 spaces generated by the analogous left-handed Clifford translations which implies that altogether we have to consider 6 spherical spaces.

In order to calculate the CMB fluctuations, we have to expand the various contributions into the vibrations on the spaces  $\mathcal{M} = \mathcal{S}^3/\Gamma$  which are determined by the regular solutions of the Helmholtz equation

$$(\Delta + E_\beta^{\mathcal{M}})\psi_\beta^{\mathcal{M},i}(q) = 0 \quad , \quad q \in \mathcal{M} \quad , \quad (2)$$

satisfying the periodicity conditions

$$\psi_\beta^{\mathcal{M},i}(\gamma_k q) = \psi_\beta^{\mathcal{M},i}(q) \quad , \quad \forall q \in \mathcal{M} \quad , \quad \forall \gamma_k \in \Gamma \quad . \quad (3)$$

Here  $\Delta$  denotes the Laplace-Beltrami operator on  $\mathcal{S}^3$ , and the eigenfunctions  $\psi_\beta^{\mathcal{M},i}(q)$  are in  $L^2(\mathcal{M}, d\mu)$  with  $d\mu$  the invariant measure on  $\mathcal{S}^3$ . The spectrum on  $\mathcal{M}$  is discrete, and the eigenvalues can be expressed in terms of the wave number  $\beta \in \mathbb{N}$  as  $E_\beta^{\mathcal{M}} = \beta^2 - 1$  and are independent of the degeneracy index  $i = 1, \dots, r^{\mathcal{M}}(\beta)$ , where  $r^{\mathcal{M}}(\beta)$  denotes the multiplicity of the mode  $\beta$ . Only for  $\mathcal{S}^3$ ,  $\beta$  takes all values in  $\mathbb{N}$ . The allowed wave numbers  $\beta$  for the above mentioned spherical manifolds are explicitly known (Ikeda 1995), see Table 1.

The relative temperature fluctuations of the CMB are caused by several effects which we shall compute within the tight-coupling approximation along the lines described in Section 2 of Aurich et al. (2004). The tight-coupling approximation leads to the Sachs-Wolfe formula (7), which incorporates the various effects to be discussed below. Furthermore, we assume here isentropic initial conditions and for the primordial power spectrum a scale-invariant Harrison-Zel'dovich spectrum

$$P_\Phi(\beta) = \frac{\alpha}{\beta(\beta^2 - 1)} \quad , \quad (4)$$

where  $\alpha$  is a normalization factor which will be determined from the CMB data such that the angular power spectrum  $\delta T_l^2$  fits the WMAP values in the range  $l = 20$  to  $l = 45$ .

## 3 COSMIC TOPOLOGY AND THE CIRCLES-IN-THE-SKY SIGNATURE

There are infinitely many multi-connected spherical space forms as described in the previous section. Aurich et al. (2005b,a) examined the angular power spectrum  $\delta T_l^2 := l(l+1)C_l/(2\pi)$  and the temperature two-point correlation function  $C(\vartheta)$  for the Poincaré dodecahedron  $\mathcal{D}$  and for many globally homogeneous spherical manifolds and found a good agreement on large scales with the WMAP data only for the binary tetrahedral, the binary octahedral, and the dodecahedral space forms. A strong suppression on large scales, as seen in the WMAP data, is obtained for the binary tetrahedral space form  $\mathcal{T}$  for  $\Omega_{\text{tot}} = 1.06\dots 1.07$ , for the

**Table 1.** The eigenvalue spectrum of the considered spherical spaces  $\mathcal{S}^3$  and  $\mathcal{S}^3/\Gamma$ .

$\mathcal{M}$	wave number spectrum $\{\beta\}$ of manifold $\mathcal{M}$	multiplicity $r^{\mathcal{M}}(\beta)$
$\mathcal{S}^3$	$\mathbb{N}$	$\beta^2$
$\mathcal{S}^3/T^*$	$\{1, 7, 9\} \cup \{2n + 1   n \geq 6\}$	$\beta \left( 2 \left[ \frac{\beta-1}{6} \right] + \left[ \frac{\beta-1}{4} \right] - \frac{\beta-3}{2} \right)$
$\mathcal{S}^3/O^*$	$\{1, 9, 13, 17, 19, 21\} \cup \{2n + 1   n \geq 12\}$	$\beta \left( \left[ \frac{\beta-1}{8} \right] + \left[ \frac{\beta-1}{6} \right] + \left[ \frac{\beta-1}{4} \right] - \frac{\beta-3}{2} \right)$
$\mathcal{S}^3/I^*$	$\{1, 13, 21, 25, 31, 33, 37, 41, 43, 45, 49, 51, 53, 55, 57\} \cup \{2n + 1, n \geq 30\}$	$\beta \left( \left[ \frac{\beta-1}{10} \right] + \left[ \frac{\beta-1}{6} \right] + \left[ \frac{\beta-1}{4} \right] - \frac{\beta-3}{2} \right)$

binary octahedral space form  $\mathcal{O}$  for  $\Omega_{\text{tot}} = 1.03\dots 1.04$ , and for the dodecahedral space form  $\mathcal{D}$  for  $\Omega_{\text{tot}} = 1.015\dots 1.02$ . This is a hint that one of these topologies could be realized in our Universe. Here  $\Omega_{\text{tot}} := \varepsilon_{\text{tot}}/\varepsilon_{\text{crit}}$  is the energy density parameter, where  $\varepsilon_{\text{tot}}$  denotes the total energy density of the universe and  $\varepsilon_{\text{crit}} := \frac{3H_0^2}{8\pi G}$  the critical energy density at the present epoch.

In order to investigate these topologies further, we perform a special search for the so-called circles-in-the-sky signature (Cornish et al. 1998) in the CMB sky maps. This topological signal is caused by the multi-connectedness of the assumed space forms. The surface of last scattering (SLS) is a 2-sphere with the observer at the centre. In multi-connected manifolds, copies of the SLS and the observer are generated by the periodicity conditions (3). If the distance between the observer and a copy of him (“mirror observer”) is smaller than the diameter of the SLS, the two SLS’s intersect. This intersection is a circle. Both the observer and the copy of the observer see this circle, but in different directions on the sky. Because there is really only one observer, this one observer should detect two circles in different directions in the microwave sky map.

For a quantitative search of these matched circles, Cornish et al. (1998) define the quantity

$$S(\rho) := \frac{\langle 2\delta T_a(\pm\phi)\delta T_b(\phi+\rho) \rangle}{\langle \delta T_a^2(\phi) + \delta T_b^2(\phi) \rangle}. \quad (5)$$

$\delta T_a(\phi)$  and  $\delta T_b(\phi)$  are the temperature fluctuations along two circles  $a$  and  $b$  on the microwave sky having the same radius. Their centres are in the directions  $\hat{n}_a$  and  $\hat{n}_b$  on the sky map. Both circles are parameterized by the angle  $\phi$ . The angle  $\rho$  gives the relative phase of these circles and  $\langle \rangle := \int_0^{2\pi} d\phi$ . By searching only for circles that are anti-phased, which corresponds to the minus sign in the nominator in (5), one restricts the search to orientable topologies, but by searching also for circles that are phased, which corresponds to the plus sign in (5), one can also detect non-orientable topologies. The  $S$  statistic can take values in the interval  $[-1, +1]$ , where  $S = +1$  corresponds to a perfect agreement between the temperature fluctuations along the two circles and  $S = -1$  to completely anticorrelated temperature fluctuations. In the next section, we shall discuss the various effects which influence the values of the  $S$  statistic.

In general, a complete search of matched circles requires a six-dimensional parameter space: four parameters for the directions  $\hat{n}_a$  and  $\hat{n}_b$  of the centres of the two circles, one parameter for the relative phase  $\rho$  of the two circles, and one parameter for the common radius of the circles. This has to

be done for both orientations of the circles. Such a search involves a huge computer time. By searching for matched circles of spherical manifolds, which are constructed either from right-handed or left-handed Clifford translations, we can lower the dimension of the parameter space and consequently reduce the computational time (Weeks et al. 2003). Since we investigate in this paper three topologies which are globally homogeneous, we have only to search for back-to-back matched circles (the circle pairs are separated by  $180^\circ$ ) which reduces the parameter space to four dimensions. Furthermore, the relative phase  $\rho$  of the circles is given. Tables 2, 3 and 4 display the dependence of the number of paired circles on the radius  $\tau_{\text{SLS}}$  of the SLS, respectively on  $\Omega_{\text{tot}}$ , for the binary polyhedral spaces  $\mathcal{T}$ ,  $\mathcal{O}$  and  $\mathcal{D}$ . In addition, the relative phases  $\rho$  and the radii of the paired circles are given. The column denoted by  $\rho$  in these Tables gives the relative phases of those circles which have to be added to the already present ones when increasing the value of  $\Omega_{\text{tot}}$ . The other circles possess the relative phases given in the preceding row. It is possible to construct these manifolds from right-handed as well as from left-handed Clifford translations leading to an identical angular power spectrum  $\delta T_l^2$  and the same correlation function  $C(\vartheta)$ , but with a reversed sign of  $\rho$  in (5) which alters the search for matched circles. Thus, one has to search for the relative phases with positive and negative sign. Furthermore, we can restrict our search to circles which are anti-phased, because the binary polyhedral spaces  $\mathcal{T}$ ,  $\mathcal{O}$  and  $\mathcal{D}$  are orientable manifolds.

A modification of the quantity  $S(\rho)$ , equation (5), is introduced by Cornish et al. (2004), but which we do not use here. Their modified quantity, see equation (1) in Cornish et al. (2004), is constructed by expanding the temperature fluctuations  $\delta T_a(\phi)$  and  $\delta T_b(\phi)$  along the two circles in Fourier series  $\delta T_{a,b}(\phi) = \sum_m T_m^{a,b} \exp(im\phi)$ . Then the coefficients  $T_m^{a,b}$  are multiplied by a factor  $\sqrt{|m|}$  leading to modified temperature fluctuations  $\delta \tilde{T}_{a,b}(\phi)$  which in turn are used in (5). This procedure enhances the small scale structure. As will be discussed below, the available microwave sky maps do not have sufficient power at small scales, especially near to the first acoustic peak. This will be demonstrated by Fig. 2 where the angular power spectrum  $\delta T_l^2$  of the CMB fluctuations is compared with the power contained in the sky maps. With the multiplication by  $\sqrt{|m|}$ , this deficit in power is only remedied in a statistical sense; the true cosmological signal of the SLS at small scales might be completely different, of course. But it is this very cosmological signal one needs for the detection of paired circles. Thus, there remains the question about how the pro-

cedure of Cornish et al. (2004) affects the topological signal in true microwave sky maps being composed of a lot of sky patches. In the next section, we propose an alternative procedure without artificially enhancing power at small scales but instead using a specially designed weight function.

One can perform a very specific search by using the information about the group  $\Gamma$  which defines the manifold  $S^3/\Gamma$ . Fixing the radius  $\tau_{\text{SLS}}$  of the SLS in the case of a homogeneous spherical manifold, the number of paired circles, their relative phases  $\rho$  and their relative orientation are determined. Only a common rotation of the whole configuration of the circles is left free which can be parameterised by three Euler angles. This fact can be used to carry out a simultaneous search over all matched circles by defining the estimator

$$\Sigma(n) := \text{sign} \left( \sum_{i=1}^n S_i \cdot |S_i| \right) \cdot \sqrt{\frac{|\sum_{i=1}^n S_i \cdot |S_i||}{n}} \quad (6)$$

$S_i$  is the  $S$  statistic of the  $i$ -th paired circles and  $n$  is their total number.  $\Sigma$  varies between  $-1$  and  $+1$ . This search has a four-dimensional parameter space: three parameters for all possible orientations of the fundamental cell and one parameter for the radius  $\tau_{\text{SLS}}$  of the SLS. The  $\Sigma$  estimator gives a better signal than the  $S$  statistic, if there are genuine matched circles; furthermore, it should be possible to detect with  $\Sigma$  smaller paired circles. Such a special search cannot be used to check all possible topologies, but if there is a hint towards a special topology, like the binary polyhedral spaces  $\mathcal{T}$ ,  $\mathcal{O}$  and  $\mathcal{D}$ , it can be carried out.

#### 4 SEARCH FOR MATCHED CIRCLES IN THE WMAP SKY MAPS

In order to perform the search for matched circles in actual sky maps, one has to take several points into account. The most important one is that one does not observe the pure signal of the temperature fluctuations on the SLS proportional to the scalar perturbation  $\Phi$ , which displays as a scalar quantity a clear sign of the topology. Even ignoring the detector noise, foreground sources and all but one secondary contribution, i. e. not excluding the integrated Sachs-Wolfe effect, one has three main contributions as revealed by the Sachs-Wolfe formula ( $\tau(\eta) := \eta_0 - \eta$ )

$$\begin{aligned} \frac{\delta T}{T}(\hat{n}) &= \sum'_{\beta \geq 3} \sum_{i=1}^{r^{\mathcal{M}(\beta)}} \\ &\left[ \left( \Phi_{\beta}^i(\eta) + \frac{\delta_{\gamma,\beta}^i(\eta)}{4} + \frac{a(\eta)V_{\gamma,\beta}^i(\eta)}{E_{\beta}} \frac{\partial}{\partial \tau} \right) \Psi_{\beta}^{\mathcal{M},i}(\tau(\eta), \theta, \phi) \right]_{\eta=\eta_{\text{SLS}}} \\ &+ 2 \sum'_{\beta \geq 3} \sum_{i=1}^{r^{\mathcal{M}(\beta)}} \int_{\eta_{\text{SLS}}}^{\eta_0} d\eta \frac{\partial \Phi_{\beta}^i(\eta)}{\partial \eta} \Psi_{\beta}^{\mathcal{M},i}(\tau(\eta), \theta, \phi) \quad (7) \end{aligned}$$

Here the summation runs only over those modes which exist for a given manifold, see Table 1. The first two terms in (7), determined by the expansion coefficients  $\Phi_{\beta}^i(\eta)$  of the gravitational potential  $\Phi$  and the intrinsic perturbation in the radiation density  $\delta_{\gamma,\beta}^i(\eta)$ , yield the effective temperature perturbation on the SLS, i. e. the ordinary Sachs-Wolfe

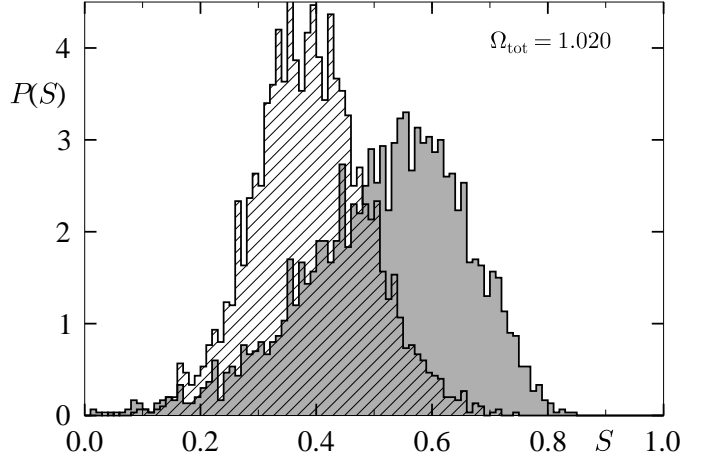


**Figure 1.** The distribution of the  $S$  values for matched pairs of circles is shown for the dodecahedral space  $\mathcal{D}$  as the grey histogram. For comparison, the distribution for  $S_{\text{max}}$  for the simply-connected space  $S^3$  is shown as a shaded histogram, where the positions of the pairs are assumed to be the same as in the dodecahedral case. The circles have a radius of  $49.8^\circ$  determined by  $\Omega_{\text{tot}} = 1.020$ . The other cosmological parameters are  $h = 0.70$ ,  $\Omega_{\text{mat}} = 0.28$  and  $\Omega_{\text{bar}} = 0.046$ .

(SW) contribution which encodes the desired topological information. The next term involving the spatial covariant divergence of the velocity field  $V_{\gamma,\beta}^i(\eta)$  is the Doppler contribution which spoils the topological signal because the projection of the velocities in the directions of the observer and the “mirror” observer are not the same. The last term, the integral over the photon path, yields the integrated Sachs-Wolfe contribution (ISW). Since the photon paths towards the observer and the mirror observer are not identified, this contribution also degrades the topological signal.

Fig. 1 demonstrates these degrading effects. The grey histogram shows the distribution of  $S(\rho)$  (see Eq. (5)) with  $\rho = 36^\circ$  for 3000 pairs of matched circles obtained from simulations of sky maps for the dodecahedral space  $\mathcal{D}$  for a fixed set of cosmological parameters. Without degrading effects, one would observe a delta-like peak at  $S = 1$ . As revealed by the grey histogram, the Doppler and ISW contributions lead to a broad distribution with a maximum around  $S = 0.6$ . The shaded histogram shows the distribution of  $S_{\text{max}} = \max_{\rho}\{S(\rho)\}$  for 3000 pairs of circles of simulations of sky maps for the simply connected space  $S^3$ . (For the positions of the circles we use the positions occurring in the dodecahedral simulations.) Since this space has no matched pairs at all, the shaded histogram provides the null hypothesis for the detection of a topological signature.

Assume for a moment that the sky map has a genuine circle signature. Then one has to scan the map for all possible orientations of the pairs of circles. The wrong guesses should lead to a distribution similar to that of the simply-connected  $S^3$ , whereas the few correct guesses are distributed as in the grey histogram. With the parameters chosen in Fig. 1, the dodecahedral space  $\mathcal{D}$  has only six pairs (see Table 2). Compared with the huge number of wrong guesses distributed as the shaded histogram, the topological signature can easily be washed out.

In order to enhance the topological signal, we apply

**Table 2.** The number of paired circles for the Poincaré dodecahedron  $\mathcal{D}$  is given in dependence on the radius  $\tau_{\text{SLS}}$  of the SLS, respectively on the total density parameter  $\Omega_{\text{tot}}$ . The parameters  $h = 0.70$  and  $\Omega_{\text{mat}} = 0.28$  are held fixed. Also the relative phases  $\rho$  of the circle pairs are shown for the right-handed (plus sign) and the left-handed (minus sign) Clifford translations as well as the radii of the circles.

$\tau_{\text{SLS}}$	$\Omega_{\text{tot}}$	# of paired circles	$\rho$	radii of the paired circles
$< 0.33$	$< 1.010$	0	-	-
$< 0.53$	$< 1.026$	6	$\pm 36^\circ$	$< 56^\circ$
$< 0.64$	$< 1.037$	16	$\pm 60^\circ$	$< 64^\circ, < 39^\circ$
$< 0.79$	$< 1.056$	22	$\pm 72^\circ$	$< 71^\circ, < 55^\circ, < 44^\circ$
$< 0.95$	$< 1.080$	37	$\pm 90^\circ$	$< 77^\circ, < 65^\circ, < 59^\circ, < 38^\circ$
$< 1.05$	$< 1.097$	43	$\pm 108^\circ$	$< 79^\circ, < 71^\circ, < 65^\circ, < 55^\circ, < 38^\circ$
$< 1.26$	$< 1.137$	53	$\pm 120^\circ$	$< 84^\circ, < 79^\circ, < 76^\circ, < 71^\circ, < 64^\circ, < 56^\circ$
$\geq 1.26$	$\geq 1.137$	59	$\pm 144^\circ$	$\geq 84^\circ, \geq 79^\circ, \geq 76^\circ, \geq 71^\circ, \geq 64^\circ, \geq 56^\circ, \geq 9^\circ$

**Table 3.** The same as in Table 2 for the binary octahedral space  $\mathcal{O}$ .

$\tau_{\text{SLS}}$	$\Omega_{\text{tot}}$	# of paired circles	$\rho$	radii of the paired circles
$< 0.40$	$< 1.015$	0	-	-
$< 0.53$	$< 1.026$	3	$\pm 45^\circ$	$< 45^\circ$
$< 0.79$	$< 1.056$	7	$\pm 60^\circ$	$< 66^\circ, < 55^\circ$
$< 1.05$	$< 1.097$	16	$\pm 90^\circ$	$< 76^\circ, < 70^\circ, < 55^\circ$
$< 1.18$	$< 1.121$	20	$\pm 120^\circ$	$< 80^\circ, < 76^\circ, < 66^\circ, < 44^\circ$
$\geq 1.18$	$\geq 1.121$	23	$\pm 135^\circ$	$\geq 80^\circ, \geq 76^\circ, \geq 66^\circ, \geq 44^\circ, \geq 6^\circ$

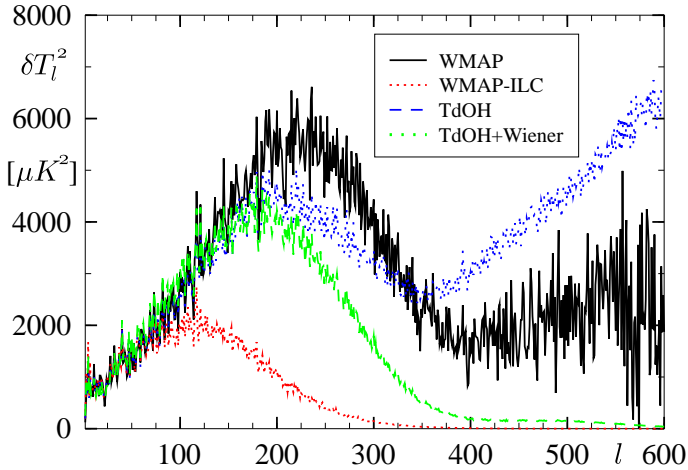


**Figure 2.** The angular power spectrum  $\delta T_l^2$  of the WMAP analysis (black) of the first year data is shown. In addition the  $\delta T_l^2$  spectra are shown obtained from the ILC map (red), the TdOH map without (blue) and with (green) a Wiener filter applied.

a special weight function to the sky maps before carrying out the search for matched pairs of circles. Furthermore, we carry out the search for all circles of a given topology simultaneously, see equation (6), which should lead to a larger signal due to the correlation.

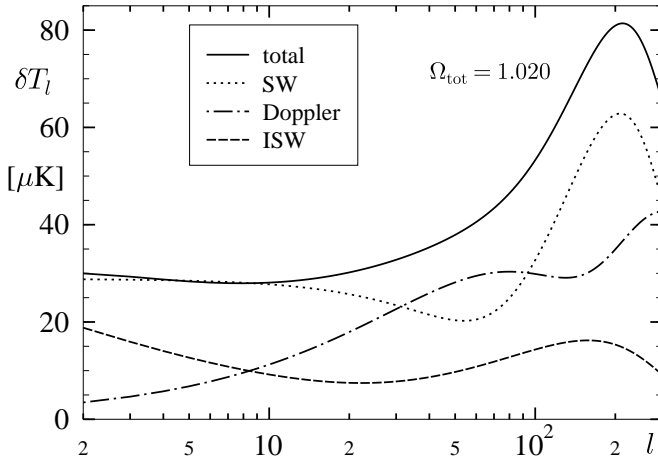
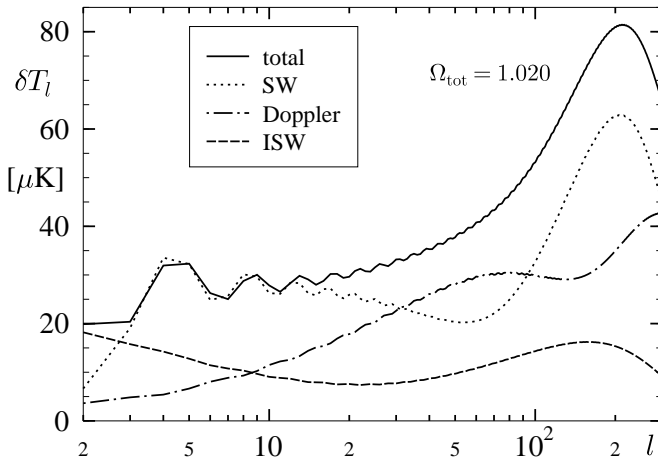
Before discussing our weight function, we describe which angular scales seem to be preferable for such a search. Only maps which cover the complete sky can be used, which restricts us to the WMAP observations. In the following we concentrate on three sky maps derived from the WMAP observation: the ILC map of Bennett et al. (2003) and the two maps of Tegmark et al. (2003) with and without the

application of a Wiener filter, respectively. The quality of these maps is discussed in (Tegmark et al. 2003; Efstathiou 2004; Eriksen et al. 2004, 2005). In order to reveal the angular scales at which these maps can be used for a circle search, we compare the angular power spectra  $\delta T_l^2$  obtained from these maps using HEALPix (HEALPix web-site: <http://healpix.jpl.nasa.gov>) with the angular power spectra obtained from a direct analysis of the WMAP first year data (Bennett et al. 2003). All four angular power spectra are shown in Fig. 2. Although it would be preferable to carry out the circle search near to the first acoustic peak, Fig. 2 reveals that the three derived maps do not have angular power spectra matching the first acoustic peak as observed in the WMAP spectrum. Only at scales larger than the first acoustic peak ( $l \lesssim 100$ ) do the four spectra agree. Thus we cannot search for the topological signature on angular scales corresponding to the first acoustic peak. Instead, we introduce our advertised weight function which takes into account only the scales with  $l \leq 70$ .

The mean value of the angular power spectrum  $\delta T_l := (l(l+1)C_l/(2\pi))^{1/2}$  is shown in Figs. 3 and 4 for the  $\mathcal{S}^3$  model and for the Poincaré dodecahedral space  $\mathcal{D}$ , respectively. We also show the individual contributions to the total temperature fluctuations as discussed below equation (7), i. e. the ordinary Sachs-Wolfe contribution (SW) encoding the topological signature, and the Doppler and the integrated Sachs-Wolfe (ISW) contributions, which both degrade the topological signal. The topological signal should be well preserved in those  $l$ -ranges, where the SW contribution dominates the other two, i. e. in the large scale  $l \lesssim 30$  region and the region around the first acoustic peak with  $100 \lesssim l \lesssim 300$ . However, as revealed by Fig. 2, neither the ILC map nor one of the TdOH maps have enough power up to  $l \simeq 300$  in order to give a reliable map for the temperature fluctuations around the first acoustic peak.

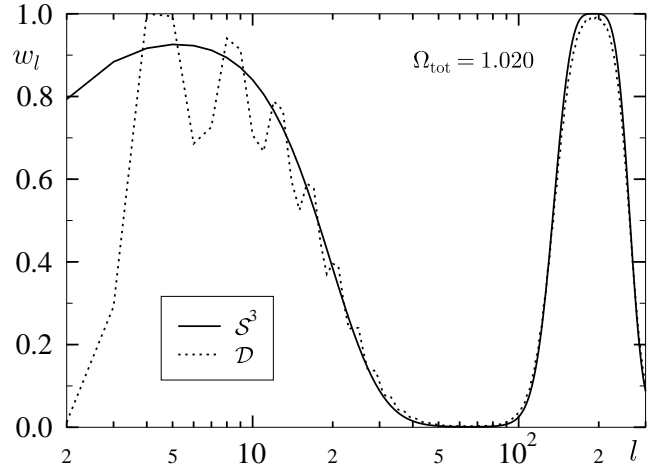
**Table 4.** The same as in Table 2 for the binary tetrahedral space  $\mathcal{T}$ .

$\tau_{\text{SLS}}$	$\Omega_{\text{tot}}$	# of paired circles	$\rho$	radii of the paired circles
$< 0.53$	$< 1.026$	0	-	-
$< 0.79$	$< 1.056$	4	$\pm 60^\circ$	$< 55^\circ$
$< 1.05$	$< 1.097$	7	$\pm 90^\circ$	$< 71^\circ, < 55^\circ$
$\geq 1.05$	$\geq 1.097$	11	$\pm 120^\circ$	$\geq 71^\circ, \geq 55^\circ, \geq 7^\circ$

**Figure 3.** The angular power spectrum  $\delta T_l$  is shown for an  $\mathcal{S}^3$  model with  $\Omega_{\text{tot}} = 1.020$  together with the ordinary Sachs-Wolfe (SW), the Doppler, and the integrated Sachs-Wolfe (ISW) contribution.**Figure 4.** The same quantities are shown as in Fig. 3, but for the Poincaré dodecahedral space  $\mathcal{D}$ .

In order to enhance the topological signal, we decompose the sky maps into the expansion coefficients  $a_{lm}$  with respect to spherical harmonics  $Y_{lm}(\hat{n})$ , multiply the coefficients  $a_{lm}$  by weight coefficients  $w_l$ , and generate from them a new map. For the weight function  $w_l$ , we choose for  $l = 2, \dots, l_{\text{cut}}$

$$w_l := \exp \left\{ -(\delta T_{\text{max}} - \delta T_l^w)^2 / \delta T_{\text{max}}^2 \right\} \quad (8)$$

**Figure 5.** The weight function  $w_l$  is shown for the  $\mathcal{S}^3$  space (full curve) and for the Poincaré dodecahedral space  $\mathcal{D}$  (dotted curve). In this figure, the cut-off is  $l_{\text{cut}} = 300$  and not  $l_{\text{cut}} = 70$  as it is set in the following computations.

with

$$\delta T_l^w := \delta T_l^{\text{SW}} - (\delta T_l^{\text{Doppler}} + \delta T_l^{\text{ISW}})$$

and

$$\delta T_{\text{max}} := \max \{ \delta T_l^w, l = 2, \dots, l_{\text{cut}} \} \quad .$$

For  $l > l_{\text{cut}}$ , we set  $w_l = 0$ . The coefficients  $\delta T_l^{\text{NSW}}$ ,  $\delta T_l^{\text{Doppler}}$  and  $\delta T_l^{\text{ISW}}$  are computed using the corresponding terms in equation (7). This weight function  $w_l$  is unity for the  $l$  value with the largest SW contribution relative to the other two contributions with  $l \leq l_{\text{cut}}$ . The modes are the more suppressed the more important the Doppler and the ISW contributions are. In Fig. 5 we show an example for the Poincaré dodecahedral space  $\mathcal{D}$  with the cosmological parameters of Fig. 1. A significant contribution comes from large scale modes with  $l \lesssim 20$ . The strong decline of  $w_l$  from  $l = 20$  to  $l = 40$  is mainly due to the growing Doppler term (see Figs. 3 and 4). Around  $l = 60..70$ , the  $w_l$ 's are close to zero because the Doppler contribution is larger than the SW contribution. Thus, we avoid a Gibb's like phenomenon by giving  $l_{\text{cut}}$  a value just within this region. In the following analysis, we use  $l_{\text{cut}} = 70$ . The contributions from the acoustic peak would also be important as revealed by Fig. 5, however, as discussed above, no reliable maps up to  $l \simeq 300$  are at hand.

The weight function  $w_l$  differs significantly for the simply-connected space  $\mathcal{S}^3$  and a multi-connected space like  $\mathcal{D}$  at small values of  $l$ . This is due to the different eigenvalue spectra of these systems (see Table 1). The modes  $l = 2$

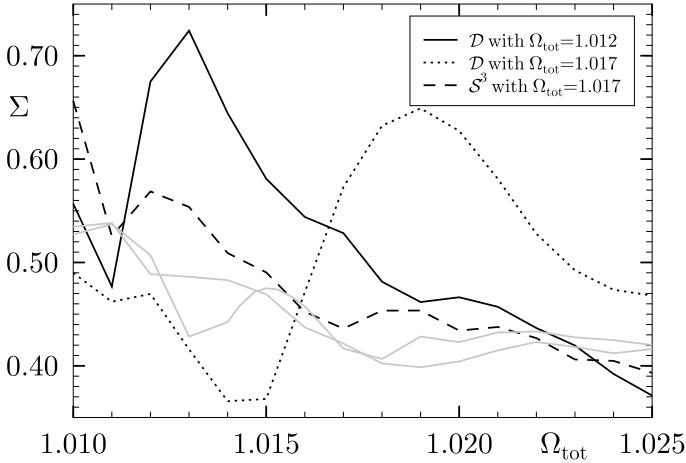


**Figure 6.** The  $\Sigma$  estimator is shown for two simulated sky maps for the Poincaré dodecahedral space  $\mathcal{D}$  and for the simply connected  $\mathcal{S}^3$ . The light grey curves show the corresponding values obtained from the Wiener filtered TdOH map for the left- and right-handed dodecahedral spaces  $\mathcal{D}$ .

and  $l = 3$  are strongly suppressed compared to the simply-connected case being a welcomed property in view of the current discussion of the validity of the maps with respect to the lowest modes (Schwarz et al. 2004). For higher values of  $l$ , the weight function  $w_l$  of multi-connected spaces fluctuates about the values for the simply-connected case.

In the following analysis, we use the specially designed  $\Sigma$  measure with respect to the space form for which the topological signal is looked for. This means that in the case of the Poincaré dodecahedral space  $\mathcal{D}$ , the weight function  $w_l$  is computed from the eigenvalues of  $\mathcal{D}$ , and all circles are used simultaneously occurring for that space for the chosen value of  $\Omega_{\text{tot}}$ . This is the best method applied up to now for the search of a given multi-connected space form. In Fig. 6 we show the results for two sky simulations for the dodecahedral space  $\mathcal{D}$  where all modes up to  $\beta = 185$  have been included which should suffice to obtain the contributions required by the weight function. One observes pronounced maxima near the values of  $\Omega_{\text{tot}}$  which are selected for the simulation. In addition, the result for a simulation of the simply-connected  $\mathcal{S}^3$  is shown displaying no large maxima. For very small circles one can by chance find a better match than for larger ones. Thus, as a general trend, one observes a decline of  $\Sigma$  with increasing values of  $\Omega_{\text{tot}}$  since then the radii of the circles increase. This behaviour is revealed by the  $\mathcal{S}^3$  simulation which has, of course, no circles at all. As grey curves the results belonging to the Wiener filtered TdOH map are shown in Fig. 6, see below. Fig. 7 compares the  $\Sigma$  estimator for the octahedral space  $\mathcal{O}$  with the one obtained from a simply-connected  $\mathcal{S}^3$  space. The result for the Wiener filtered TdOH map is also shown. This demonstrates that our  $\Sigma$  measure yields a sufficiently large topological signal despite the “contaminating” Doppler and ISW contributions.

In the considered interval of  $\Omega_{\text{tot}}$ , the Poincaré dodecahedral space  $\mathcal{D}$  produces six matched pairs of circles on the sky (see Table 2). However, with increasing values of  $\Omega_{\text{tot}}$ , the number of pairs of circles increases until the maximal possible number of 59 is reached. In general, the maximal

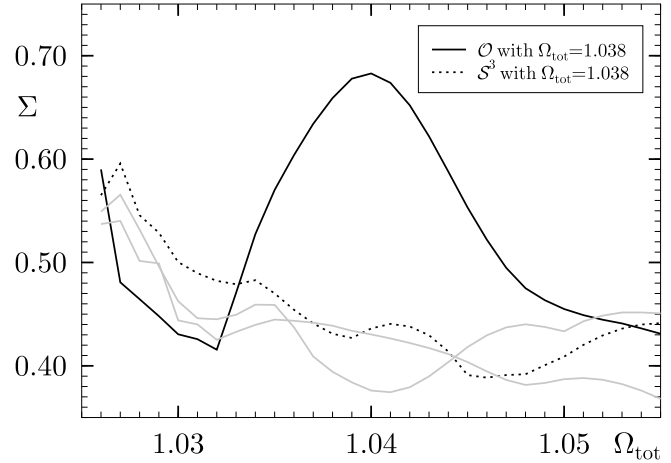


**Figure 7.** The  $\Sigma$  estimator is shown obtained from simulated sky maps for the binary octahedral space  $\mathcal{O}$  and for the simply connected  $\mathcal{S}^3$ . The light grey curves show the corresponding values obtained from the Wiener filtered TdOH map for the left- and right-handed binary octahedral spaces  $\mathcal{O}$ .

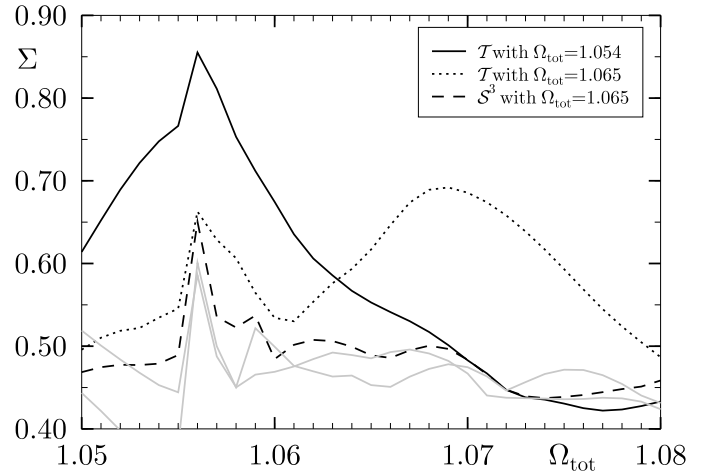


**Figure 8.** The  $\Sigma$  estimator is shown for two simulated sky maps for the binary tetrahedral space  $\mathcal{T}$  and for the simply connected  $\mathcal{S}^3$ . The light grey curves show the corresponding values obtained from the Wiener filtered TdOH map for the left- and right-handed binary tetrahedral spaces  $\mathcal{T}$ .

number of paired circles for a manifold  $\mathcal{S}^3/\Gamma$  is  $\frac{N}{2} - 1$ , where  $N$  is the order of the group. At those values of  $\Omega_{\text{tot}}$ , where the number of pairs of circles makes a jump, the  $\Sigma$  estimator jumps accordingly to larger values, which is thus not a sign of the detection of a multi-connected space form, but simply an artefact of the increasing contributing number of pairs to the  $\Sigma$  estimator. This is the case for the binary tetrahedral space  $\mathcal{T}$  at  $\Omega_{\text{tot}} = 1.056$  where the number of circle pairs jumps from 4 to 7 (see Table 4). In Fig. 8 the  $\Sigma$  estimator is shown for two sky simulations for the binary tetrahedral space  $\mathcal{T}$  having a value of  $\Omega_{\text{tot}} = 1.054$  and  $\Omega_{\text{tot}} = 1.065$ , respectively. Both show a maximum near to the expected value of  $\Omega_{\text{tot}}$ , but in addition a superimposed peak at  $\Omega_{\text{tot}} = 1.056$  is visible where the number of circle pairs jumps from 4 to 7. The same peak is seen in the  $\mathcal{S}^3$  simulation which has

no matched pairs of circles. As in Fig. 6, the grey curves display the results belonging to the Wiener filtered TdOH map. (The peak at  $\Omega_{\text{tot}} = 1.056$  is also seen in Figs. 13 and 14.)

Now, we apply the  $\Sigma$  estimator to the Poincaré dodecahedral space  $\mathcal{D}$ , the binary octahedral space  $\mathcal{O}$ , and the binary tetrahedral space  $\mathcal{T}$  using three sky maps obtained from the WMAP measurements (Bennett et al. 2003). The maps are constructed using different combinations of the data obtained in different frequency bands in order to suppress foreground sources. Different combinations are used for different sky patches. This is not ideal for the search of pairs of circles, since this leads to an inhomogeneous structure in the maps. The  $\Sigma$  estimator correlates the values on the circles which are then obtained by different combinations of the original data. The WMAP team explicitly states that their ILC map should not be used for cosmological studies. But due to a lack of an alternative, we apply, with this drawback in mind, the  $\Sigma$  estimator to the ILC map produced by the WMAP team (Bennett et al. 2003), and to the two maps of Tegmark et al. (2003).

In Figs. 9 and 10, the results for the  $\Sigma$  estimator are shown for the Poincaré dodecahedral space  $\mathcal{D}$  for the right- and left-handed space form, respectively. For the dodecahedral space  $\mathcal{D}$ , the best match to the angular power spectrum measured by WMAP is obtained around  $\Omega_{\text{tot}} = 1.018$  in Aurich et al. (2005a). Is there something special in Figs. 9 and 10 near to this value of  $\Omega_{\text{tot}}$ ? Whereas the left-handed variant shown in Fig. 10 displays only the smooth decline of  $\Sigma$  due to the increasing size of the circles with increasing values of  $\Omega_{\text{tot}}$ , the right-handed space form shown in Fig. 9 displays a clear maximum around  $\Omega_{\text{tot}} = 1.015$  in all 3 maps which is particularly distinct in the two maps of Tegmark et al. (2003). One is tempted to interpret the peak at  $\Omega_{\text{tot}} = 1.015$  as an indication that the shape of the universe is that of the right-handed Poincaré dodecahedron  $\mathcal{D}$ . However, the maximum seen in Fig. 9 is far less pronounced than the maxima obtained from our simulations of sky maps for the dodecahedral space  $\mathcal{D}$ , as can be seen by a comparison with Fig. 6 where the simulations (full and dotted curves) are presented for two different  $\Omega_{\text{tot}}$ -values together with the Wiener filtered TdOH values (grey curves). There, one observes that the height of the maximum is of the same order as the amplitude of the  $\mathcal{S}^3$  simulation possessing no matched circle pairs. However, these simulations are not based on a patchwork of sky maps, and it is expected that such a patchwork degrades the signal for a multi-connected space. But since it is unknown by how much the signal is degraded, we cannot draw firm conclusions from this structure at this moment due to the limited quality of present CMB data.

A possible hint for the left-handed dodecahedral space  $\mathcal{D}$  is found by Roukema et al. (2004) who find a slight signal for six circle pairs with  $11 \pm 1^\circ$  in the ILC map which is not revealed distinctly in Fig. 10.

The  $\Sigma$  estimator is shown for the right- and left-handed binary octahedral spaces  $\mathcal{O}$  in Figs. 11 and 12, respectively. For this space form, the best match to the WMAP angular power spectrum is obtained for values around  $\Omega_{\text{tot}} = 1.038$  (Aurich et al. 2005a). The right-handed space displays only the decrease due to the increasing size of the circles. The left-handed case displays a minimum near  $\Omega_{\text{tot}} = 1.04$  and

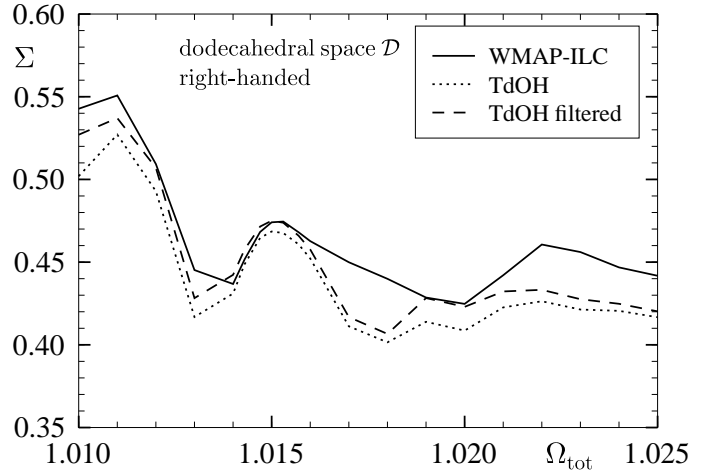


**Figure 9.** The results for the  $\Sigma$  estimator are shown evaluated for the right-handed Poincaré dodecahedral space  $\mathcal{D}$  for the ILC map and the two maps of Tegmark et al. (2003).

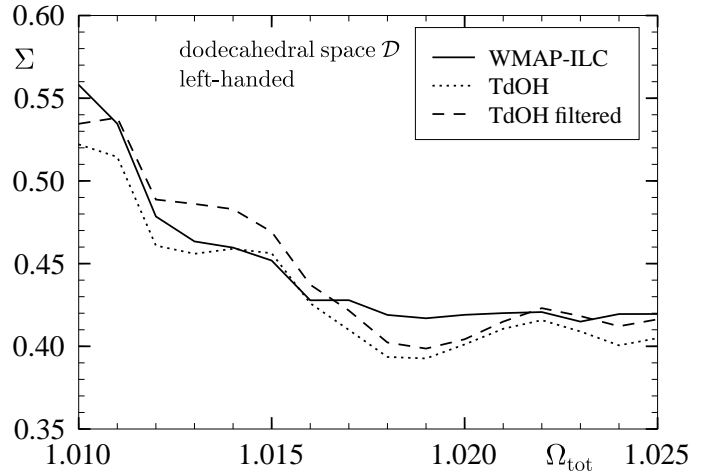


**Figure 10.** The same as in Fig. 9 is shown for the left-handed Poincaré dodecahedral space  $\mathcal{D}$ .

$\Sigma$  increases for higher values of  $\Omega_{\text{tot}}$  only to values typical of the  $\mathcal{S}^3$  simulation.

Figs. 13 and 14 show the  $\Sigma$  estimator for the tetrahedral space  $\mathcal{T}$  again for the right- and the left-handed variant, respectively. In Aurich et al. (2005a) it is found that the suppression of large scale power agrees with the WMAP measurement for  $\Omega_{\text{tot}}$  in the range  $1.06 \dots 1.07$ . The large peak observed around  $\Omega_{\text{tot}} = 1.056$  is caused by the increase of the number of circle pairs which jumps from 4 to 7 (see Table 4). The right-handed space form displays large values around  $\Omega_{\text{tot}} \simeq 1.068$ . As in the case of the dodecahedron, the maximum is far less pronounced than in the simulation of a  $\mathcal{T}$  sky as revealed by Fig. 8, and the remarks concerning the dodecahedron's maximum applies also to this case.

## 5 CONCLUSION

We performed a thorough search for a circle-in-the-sky signature in CMB maps under the hypothesis that the topol-

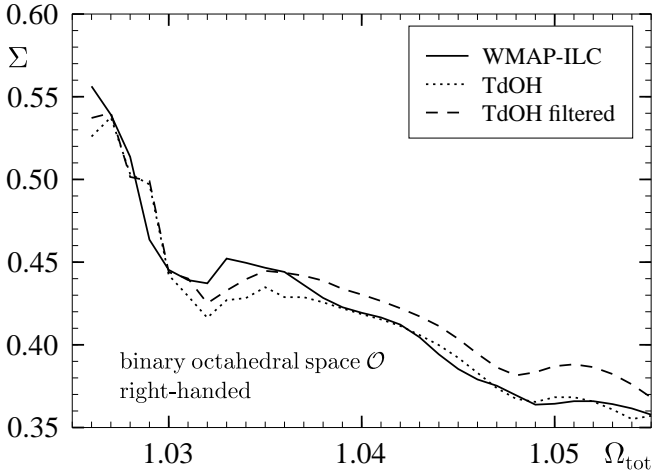


**Figure 11.** The same as in Fig. 9 is shown for the right-handed binary octahedral space  $\mathcal{O}$ .

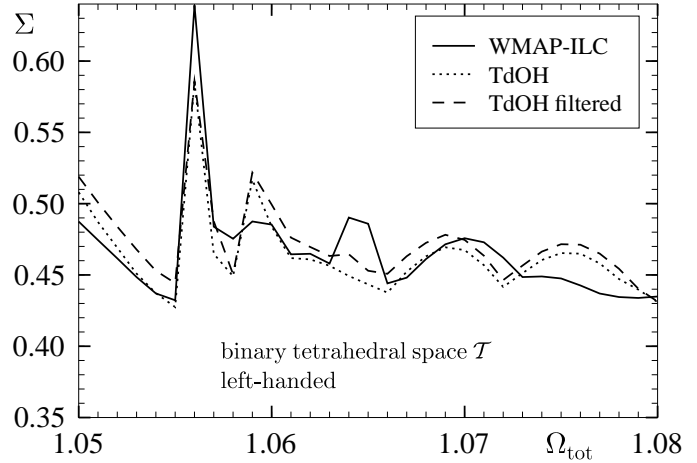


**Figure 14.** The same as in Fig. 9 is shown for the left-handed binary tetrahedral space  $\mathcal{T}$ .

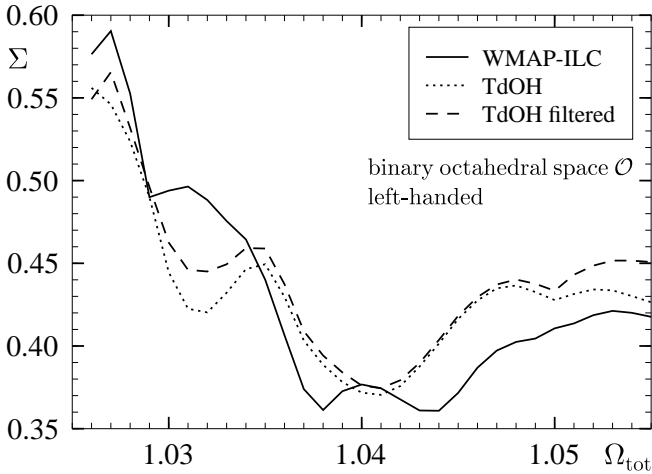


**Figure 12.** The same as in Fig. 9 is shown for the left-handed binary octahedral space  $\mathcal{O}$ .

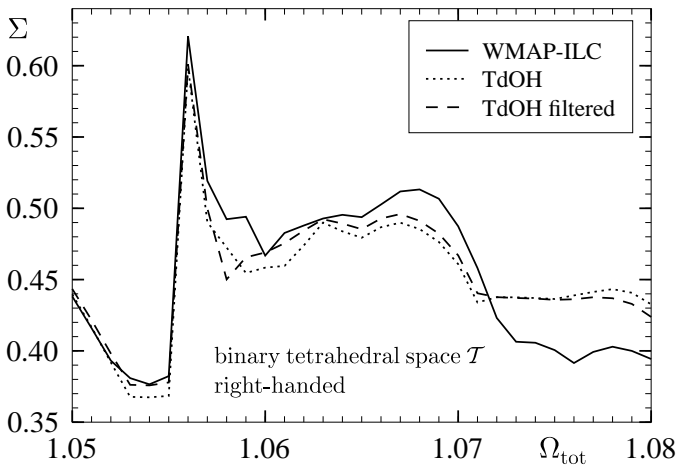


**Figure 13.** The same as in Fig. 9 is shown for the right-handed binary tetrahedral space  $\mathcal{T}$ .

ogy of the universe is given by one of the 3 spherical spaces known as  $\mathcal{D}$ ,  $\mathcal{T}$ , and  $\mathcal{O}$ . To this purpose, we introduced the  $\Sigma$  estimator (6) which is applied to filtered sky maps using the weight function (8) in order to enhance the ordinary Sachs-Wolfe contribution. A possible signal was found in the case of the right-handed Poincaré dodecahedral space  $\mathcal{D}$  for  $\Omega_{\text{tot}} \simeq 1.015$ , see Fig. 9, which can be interpreted as a hint that our universe possesses the topology of  $\mathcal{D}$ . A similar possible signal occurred in the case of the right-handed binary tetrahedral space around  $\Omega_{\text{tot}} \simeq 1.068$ , see Fig. 13. However, one must keep in mind that all three sky maps, derived from the WMAP measurements in five frequency bands, are a patchwork and thus possess a complicated signal to noise behaviour. Since the use of these incomplete sky maps certainly degrades a possible topological signal, and in order to avoid a “false negative”, we can only report our findings without drawing a final conclusion about the true topology of the Universe. Furthermore, we believe that Cornish et al. (2004) overstate their result of not finding paired circles since they also rely on the same CMB data. The question whether our Universe possesses a non-trivial topology is to our opinion not yet decided.

## REFERENCES

- Aurich R., Lustig S., Steiner F., 2005a, *Class. Quantum Grav.*, 22, 3443  
 Aurich R., Lustig S., Steiner F., 2005b, *Class. Quantum Grav.*, 22, 2061  
 Aurich R., Lustig S., Steiner F., Then H., 2004, *Class. Quantum Grav.*, 21, 4901  
 Bennett C. L. et al. 2003, *Astrophys. J. Supp.*, 148, 1  
 Cornish N. J., Spergel D. N., Starkman G. D., 1998, *Class. Quantum Grav.*, 15, 2657  
 Cornish N. J., Spergel D. N., Starkman G. D., Komatsu E., 2004, *Phys. Rev. Lett.*, 92, 201302  
 Efstathiou G., 2004, *Mon. Not. R. Astron. Soc.*, 348, 885  
 Eriksen H. K., Banday A. J., Górski K. M., Lilje P. B., 2004, *Astrophys. J.*, 612, 633  
 Eriksen H. K., Banday A. J., Górski K. M., Lilje P. B., 2005, *astro-ph/0508196*

- Gausmann E., Lehoucq R., Luminet J., Uzan J.-P., Weeks J., 2001, *Class. Quantum Grav.* , 18, 5155
- Ikeda A., 1995, *Kodai Math. J.*, 18, 57
- Lachièze-Rey M., Luminet J., 1995, *Physics Report*, 254, 135
- Levin J., 2002, *Physics Report*, 365, 251
- Luminet J., Weeks J. R., Riazuelo A., Lehoucq R., Uzan J., 2003, *Nature* , 425, 593
- Roukema B. F., Lew B., Cechowska M., Marecki A., Bajtlik S., 2004, *Astron. & Astrophys.* , 423, 821
- Schwarz D. J., Starkman G. D., Huterer D., Copi C. J., 2004, *Phys. Rev. Lett.* , 93, 221301
- Smoot G. F. et al. 1992, *Astrophys. J. Lett.* , 396, L1
- Tegmark M., de Oliveira-Costa A., Hamilton A. J. S., 2003, *Phys. Rev. D* , 68, 123523
- Threlfall W., Seifert H., 1930, *Math. Annalen*, 104, 1
- Threlfall W., Seifert H., 1932, *Math. Annalen*, 107, 543
- Weeks J., Lehoucq R., Uzan J., 2003, *Classical and Quantum Gravity*, 20, 1529
- Wolf J. A., 1974, *Spaces of constant curvature*. Publish or Perish Boston, Mass.